Spectroscopic Analysis of the Trinuclear Cluster in the Fet3 Protein from Yeast, a Multinuclear Copper Oxidase†

Ninian J. Blackburn,‡ Martina Ralle,‡ Richard Hassett,§ and Daniel J. Kosman*,§

Department of Biochemistry and Molecular Biology, Oregon Graduate Institute, 20000 Northwest Walker Road, Beaverton, Oregon 97006, and Department of Biochemistry, School of Medicine and Biomedical Sciences, State University of New York at Buffalo, Buffalo, New York 14214

Received October 7, 1999; Revised Manuscript Received December 9, 1999

ABSTRACT: The Fet3 protein (Fet3p) is a multinuclear copper oxidase essential for high-affinity iron uptake in yeast. Fet3p contains one type 1, one type 2, and a strongly antiferromagnetically coupled binuclear Cu(II)−Cu(II) type 3 copper. The type 2 and type 3 sites constitute a structurally distinct trinuclear cluster at which dioxygen is reduced to water. In Fet3p, as in ceruloplasmin, Fe(II) is oxidized to Fe(III) at the type 1 copper; this is the ferroxidase reaction that is fundamental to the physiologic function of these two enzymes. Using site-directed mutagenesis, we have generated type 1-depleted (T1D), type 2-depleted (T2D), and T1D/T2D mutants. None were active in the essential ferroxidase reaction catalyzed by Fet3p. However, the spectroscopic signatures of the remaining Cu(II) sites in any one of the three mutants were indistinguishable from those exhibited by the wild type. Although the native protein and the T1D mutant were isolated in the completely oxidized Cu(II) form, the T2D and T1D/T2D mutants were found to be completely reduced. This result is consistent with the essential role of the type 2 copper in dioxygen turnover, and with the suggestions that cuprous ion is the valence state of intracellular copper. Although stable to dioxygen, the Cu(I) sites in both proteins were readily oxidized by hydrogen peroxide. The double mutant was extensively analyzed by X-ray absorption spectroscopy. Edge and near-edge features clearly distinguished the oxidized from the reduced form of the binuclear cluster. EXAFS was strongly consistent with the expected coordination of each type 3 copper by three histidine imidazoles. Also, copper scattering was observed in the oxidized cluster along with scattering from a ligand corresponding to a bridging oxygen. The data derived from the reduced cluster indicated that the bridge was absent in this redox state. In the reduced form of the double mutant, an N/O ligand was apparent that was not seen in the reduced form of the T1D protein. This ligand in T1D/T2D could be either the remaining type 2 copper imidazole ligand (from His416) or a water molecule that could be stabilized at the type 3 cluster by H-bonding to this side chain. If present in the native protein, this H_2O could provide acid catalysis of dioxygen reduction at the reduced trinuclear center.

The Fet3 protein (Fet3p) from the budding yeast, *Saccharomyces cerevisiae*, is required for the high-affinity iron uptake in this organism (*1*−*4*). Fet3p is a type 2 plasma membrane protein; in the yeast plasma membrane, it appears to be directly associated with the high-affinity iron permease, Ftr1p (*5*, *6*). Fet3p catalyzes a ferroxidase reaction that is then coupled to the transport of iron into the yeast cell through Ftr1p. This ferroxidase reaction, illustrated in eq 1

$$4Fe(II) + O_2 + 4H^+ \rightarrow 4Fe(III) + 2H_2O \qquad (1)$$

is also an essential reaction in mammalian iron homeostasis (*7*, *8*); in mammals, the serum protein, ceruloplasmin (Cp) (*7*−*10*), catalyzes this reaction. Both Fet3p (*11*, *12*) and ceruloplasmin (*13*, *14*) are multinuclear copper oxidases, enzymes that couple the four-electron reduction of dioxygen (to water) to the oxidation of four, one-electron equivalents of the reducing substrate (*15*, *16*). Among these copper oxidases, which include also ascorbate oxidase (AO) and laccase (Lac), only Fet3p and Cp can use Fe(II) as the substrate (*2*, *9*, *10*, *12*). Thus, only Fet3p and ceruloplasmin support the ferroxidase reaction shown in eq 1.

As a class, multinuclear copper oxidases have three distinct types of copper sites (*16*, *17*). These include one type 1 (T1), or blue, Cu(II) site that is characterized by an intense Cys-S π to Cu^{2+} $d_{x^2-y^2}$ charge-transfer adsorption at ∼600 nm (ϵ = 4000−6000 M^{-1} cm^{-1}) and a correspondingly small parallel copper hyperfine coupling that is evident in the EPR spectrum ($A_{||} = 43-95 \times 10^{-4}$ cm^{-1}). These values for Fet3p are 5500 M^{-1} cm^{-1} and 91 × 10^{-4} cm^{-1}, respectively (*11*, *12*). These enzymes also contain a trinuclear copper cluster that includes one type 2 (T2) and one type 3 (T3) binuclear site. Type 2 Cu(II) exhibits the weak d−d absorbance and normal copper hyperfine coupling typical of (pseudo)square-planar Cu(II) complexes containing nitrogenous and/or

† This work was supported by National Institutes of Health Grant DK53820 (D.J.K.) and Grant GM54803 (N.J.B.) from the U.S. Public Health Service.

* To whom correspondence should be addressed: 140 Farber Hall, 3435 Main St., Buffalo, NY 14214. Phone: (716) 829-2842. Fax: (716) 829-2661. E-mail: camkos@acsu.buffalo.edu.

‡ Oregon Graduate Institute.

§ State University of New York at Buffalo.

10.1021/bi992334a CCC: $19.00
Published on Web 02/09/2000

Scheme 1

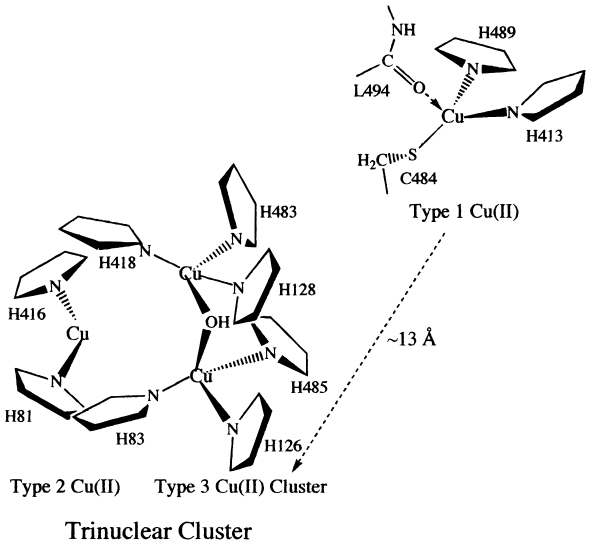

oxygenous ligands (for Fet3p, $A_{||} = 190 \times 10^{-4}$ cm^{-1}). The binuclear Cu(II) cluster is diamagnetic due to strong antiferromagnetic coupling associated with a bridging oxygen (-OH) atom; however, its presence is reflected in a relatively strong transition at 330 nm (for Fet3p, $\epsilon = 5000$ M^{-1} cm^{-1}) that is apparent as a shoulder on the protein absorbance at 280 nm.

The crystal structures of human ceruloplasmin (hCp)[1] (*13*, *14*), AO (*18*, *19*), and Lac (*20*) have revealed the spatial relationship between the three copper sites. The type 1 copper site is separated from the trinuclear cluster by ~13 Å, while the three copper atoms in the trinuclear cluster form a nearly isosceles triangle, 3.5−4.0 Å on a side. The structures also confirmed the protein side chain ligand assignments indicated by solution studies and sequence alignments among the members of this protein family. Scheme 1 illustrates a model of the trinuclear cluster in Fet3p based on the hCp and AO structures and these alignments, and its spatial relationship to the type 1 copper site. This latter Cu(II) is the site of entry of electrons from the reducing substrate, Fe(II) in the case of Fet3p and Cp, while dioxygen reduction occurs at the trinuclear cluster.

Spectral analysis of a specific copper site in a multinuclear oxidase is complicated by the presence of the other sites. This is particularly true of X-ray absorbance, in which case all four copper atoms would contribute to both the copper edge absorption and the extended fine structure due to backscattering from neighboring atoms (*21*). On the other hand, EXAFS has the potential of providing molecular and atom-level details of the coordination sites in metalloproteins and is the only spectral technique that is directly useful in the structural characterization of the diamagnetic type 3 binuclear cluster, particularly in its reduced state which exhibits no optical transitions.

The Fet3p system offers a unique opportunity to employ XAS in the study of this site due to the ease of constructing site-directed mutants in the gene encoding Fet3p, *FET3*, and then in producing the recombinant mutant proteins in yeast in a soluble form (*11*, *12*). Here, on the basis of the model of the Fet3 protein illustrated in Scheme 1, we have sequentially deleted putative copper ligands to the type 1 and type 2 copper atoms, thus generating a trio of mutant proteins lacking one or more copper atoms, i.e., T1D, T2D, and T1D/T2D Fet3p. This latter mutant protein, which contains only the type 3 binuclear cluster, is unique among the multi-copper oxidases in that this site has never been isolated in this manner previously. With this protein, we have been able to use XAS to delineate the structure of the oxidized and reduced forms of this site. The results both are consistent with and extend the current model for how the type 3 cluster participates in the reduction of dioxygen. Furthermore, the success of the mutagenesis itself strongly supports the ligand assignments in Fet3p given in Scheme 1.

EXPERIMENTAL PROCEDURES

Expression and Purification of Soluble Fet3p. Strain M2* carrying plasmid pDY148 was used as the expression system for the production of soluble Fet3p. Strain M2* is *MAT*α *trp1−63 leu2−3,112 gcn4−101 his3−609 ura3−52 AFT1−1^{up}* (*22*). The *AFT1−1^{up}* allele encodes a dominant, gain-of-function mutant of the Aft1 protein, the transactivator of the genes of the iron regulon, including *FET3* (*23*). Plasmid pDY148 is a 2μ vector that carries a recombinant *FET3* effectively truncated at nucleotide 1666 (at amino acid residue 555, below). This truncation removed the apparent membrane-spanning domain found in the C-terminal region that is included in residues 559−586; as a consequence, this Fet3p was secreted directly into the growth medium rather than being retained in the plasma membrane. Culture growth and mutant protein purification were performed as has been described in detail for the wild-type protein (*12*).

Construction of Fet3p Mutants. Mutant *FET3* alleles were constructed directly in pDY148 by site-directed mutagenesis using the QuickChange kit from Stratagene. Briefly, complementary primers encoding the Cys484Ser mutation at the type 1 copper site and those encoding the His81Gln mutation at the type 2 copper site were used in PCR amplification of the vector. Following amplification of the mutant-encoding vectors in bacteria, the *FET3* sequences were confirmed by dideoxy sequencing (Sequenase 2.0) and the vectors transformed into yeast host strain M2*. The T1D/T2D mutant allele was generated by a second pass through the QuickChange procedure using the T1D *FET3* as a template.

Analytical and Spectral Methods. The protein concentration was determined by two independent assays, a standard dye-binding one (Bradford) (*24*) and a redox-based one (copper/biscinchoninic acid) (*25*). The copper content was determined by flameless atomic absorption spectrophotometry on a Perkin-Elmer model 1100 instrument equipped with a model 700 graphite furnace. Fe(II) oxidation to Fe(III) (the ferroxidase reaction) was followed spectrophotometrically at 315 nm ($\Delta\epsilon = 2200$ M^{-1} cm^{-1}) (*26*). Absorbance spectra were recorded on a Beckman model 620B instrument at room temperature. EPR spectra were obtained at 77 and 20 K on a Bruker model 300E spectrometer operating at 9.5 GHz (X-band).

[1] Abbreviations: hCp, human ceruloplasmin; AO, ascorbate acid oxidase; Lac, laccase; XAS, X-ray absorption spectroscopy; EXAFS, extended X-ray absorption fine structure; EPR, electron paramagnetic resonance; FF, Fourier-filtered; ESEEM, electron spin-echo envelope modulation; MCD, magnetic circular dichroism.

X-ray Absorption (XAS) Data Collection and Analysis. XAS data were collected at the Stanford Synchrotron Radiation Laboratory (SSRL) on beam line 7.3, operating at 3.0 GeV with beam currents between 100 and 50 mA. A Si220 monochromator with 1.2 mm slits was used to provide monochromatic radiation in the 8.8−10 keV energy range. The monochromator was detuned 50% to reject harmonics. The protein samples were measured as frozen glasses in 25% glycerol at 11−14 K in fluorescence mode using a 13-element Ge detector. To avoid detector saturation, the count rate of each detector channel was kept below 100 kHz by adjusting the hutch entrance slits, or by moving the detector in or out from the cryostat windows. Under these conditions, no dead-time correction was necessary. The summed data for each detector were then inspected, and only those channels that gave high-quality backgrounds free from glitches, dropouts, or scatter peaks were included in the final average.

Raw data were averaged, background subtracted, and normalized to the smoothly varying background atomic absorption using the EXAFS data reduction package EXAFSPAK (*27*). Energy calibration was achieved by reference to the first inflection point of a copper foil (8980.3 eV) placed between the second and third ion chambers. In any series of scans, the measured energy of the first inflection of the copper foil spectrum varied by less than 1 eV. Averaged EXAFS data were referenced to the copper calibration of the first scan of a series, since the energy drift in any series of scans was too small to perturb the EXAFS oscillations.

Data analysis was carried out with the least-squares curve-fitting program EXCURV98 which utilizes full curved-wave calculations as described by Gurman and co-workers (*28*−*30*). The application to metalloprotein systems, and particularly the treatment of imidazole rings from histidine residues, of multiple scattering analysis has been described in detail (*31*−*33*). First-shell Fourier-filtered data were used to estimate the splitting of the first shell. Next, the single and multiple scattering contributions of the imidazole outer shells were included. To ensure accuracy, the outer shell distances and imidazole ring geometry were generated by molecular modeling, using the builder module of INSIGHT 3.0 (Molecular Simulations Inc., San Diego, CA). A model of the copper center with a single coordinated imidazole was first built and the Cu−N first-shell bond length adjusted to be close to the EXAFS-derived bond length (as determined by first-shell analysis using Fourier-filtered data). This model was then converted into molecular coordinates and read into EXCURV98 to provide a single Cu−imidazole unit with the correct geometry. The coordination number of this unit was then set within the EXAFS program. Least-squares minimization was performed, varying only the Cu−N(imid) first-shell distance (R), its Debye−Waller factor (DW, $2\sigma_i^2$), and the E_O, the photoelectron threshold energy. Finally, the C_β and C_γ/N_γ shells were allowed to minimize, but were constrained so as to remain within 0.1 Å of the initially chosen geometry. This latter process was found to be crucial in obtaining good fits to all data reported herein, and almost certainly reflects the real tendency of coordinated imidazole rings to distort from ideal geometries in response to tertiary constraints of the polypeptide fold. These ideal geometries were used as a starting point but were then allowed to float with restraint (±10°) in the multiple scattering analysis. The angle refinement was correlated with the Debye−Waller term for that shell, and became increasingly less sensitive as the angle decreased from 180°. Coordination numbers were fixed at values consistent with the crystallographic descriptions of hCp (*13*, *14*), AO (*18*, *19*), and Lac (*20*), but were allowed to float in some fits to test the consistency between spectroscopic and crystallographic results. In the latter case, the coordination numbers were constrained so as to produce DW factors within reasonable limits (first shell, $0 < 2\sigma^2 < 0.015$; second shell ≥ first shell). The goodness of fit was judged by reference to the parameter F, defined as

$$F^2 = \frac{1}{N}\sum_{i=1}^{n} k^6(\text{data}_i - \text{model}_i)^2$$

Scheme 2

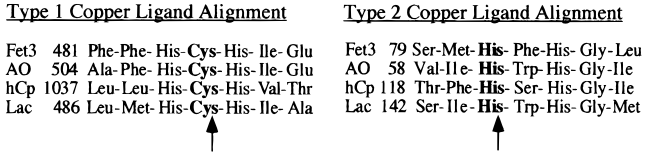

RESULTS

Production of Mutant Fet3 Proteins. Plasmid pDY148 is a high-copy vector that carries a recombinant *FET3* gene truncated at nucleotide 1668 or at residue 555 in the wild-type Fet3p sequence (*3*). This truncation removed the apparent membrane-spanning domain found in the C-terminal region that is included in residues 559−586 and which anchors the endogenous Fet3p in the yeast plasma membrane in association with the high-affinity iron permease, Ftr1p (*5*). As a result of this truncation, this recombinant Fet3p, although produced and processed normally in the vesicular trafficking pathway, is secreted into the growth medium from which it can be readily purified (*11*, *12*).

The T1D, T2D, and T1D/T2D mutants used in these studies were derived from the pDY148 system by site-directed mutagenesis. The single-point mutations in the Fet3 proteins that were produced were based on the sequence alignments among multi-copper oxidases shown in Scheme 2 that highlight residues that serve as ligands to either the type 1 or type 2 copper atoms in these proteins. To construct the T1D mutant, a Cys484Ser substitution was encoded (a G to C transversion at nucleotide 1451), while for the T2D mutant, a His81Gln substitution was encoded (a T to A transversion at nucleotide 243). The gene encoding the T1D mutant was subsequently used as a template for production of the T1D/T2D double mutant in a second round of mutagenesis. In all cases, the mutant-encoding sequences were confirmed by sequence analysis. The fact that the single substitutions that were introduced did indeed result in the loss of a specific copper site strongly supported the alignments shown in Scheme 2 (and the model in Scheme 1). The yields of the three mutant proteins were comparable to that of the wild type (~5 mg of Fet3 protein isolated per liter of growth medium) (*12*).

Catalytic, Spectral, and Redox Properties of the Fet3 Mutant Proteins. None of the mutant proteins were enzymatically active with either *o*-dianisidine or Fe(II) as the reducing substrate (data not shown). In other respects, in their fully oxidized states, ensured by treatment with peroxide (*11*,

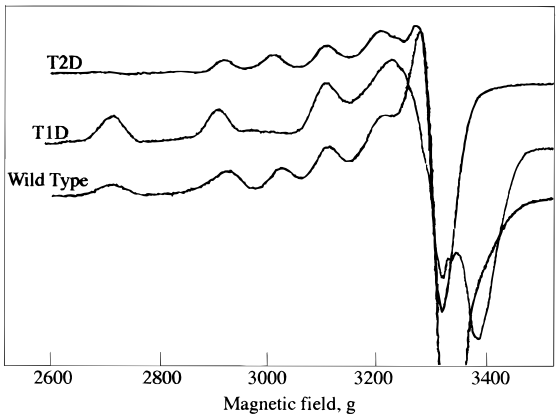

FIGURE 1: Electron paramagnetic resonance spectra of wild-type and the T1D and T2D mutants of Fet3p. Spectra were obtained at a microwave frequency of 9.5 ± 0.05 GHz and 120 K. The samples were prepared in 25% v/v ethylene glycol/50 mM MES buffer (pH 6.0). The instrument settings were constant: microwave power, 10 mW; modulation frequency, 100 kHz; modulation amplitude, 10 G; time constant, 0.02 s; and sweep time, 60 s.

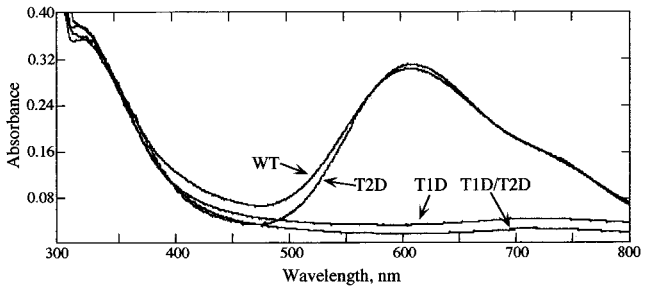

FIGURE 2: Absorbance spectra of wild-type and the T1D, T2D, and T1D/T2D mutants of Fet3p. All samples were prepared in 50 mM MES buffer (pH 6.0). Spectra were recorded following treatment of the samples with 0.5 mM hydrogen peroxide to ensure that all copper atoms present were in the cupric state (see Experimental Procedures).

12), they had spectral properties consistent with the Cu(II) sites remaining in the protein. Thus, the T1D protein exhibited the EPR spectrum previously assigned to the type 2 Cu(II) in Fet3p (Figure 1, T1D; $g_{||} = 2.24$, $A_{||} = 195 \times 10^{-4}$ cm^{-1}), while it lacked the intense blue color and absorbance at 607 nm due to the type 1 Cu(II) in this multicopper oxidase (Figure 2, T1D). In contrast, the EPR spectrum of the T2D mutant exhibited only the narrow copper hyperfine coupling due to the type 1 Cu(II) (Figure 1, T2D; $g_{||} = 2.19$, $A_{||} = 89 \times 10^{-4}$ cm^{-1}) and, correspondingly, retained the characteristic intense ~600 nm absorbance of a type 1 Cu(II) (Figure 2). Both single mutants exhibited the type 3 Cu(II) absorbance at 330 nm (~5000 M^{-1} cm^{-1}) as well as weak absorbance at ~720 nm (Figure 2). For reference, the wild-type protein had a $g_{||}$ of 2.20 and an $A_{||}$ of 91 × 10^{-4} cm^{-1} [type 1 Cu(II)] and a $g_{||}$ of 2.26 and an $A_{||}$ of 190 × 10^{-4} cm^{-1} [type 2 Cu(II)] (Figure 1 and refs *11* and *12*), indicating that in either mutant protein there were only subtle differences in structure at the remaining paramagnetic Cu(II) site.

The T1D/T2D mutant was apparently diamagnetic since it gave no EPR spectrum under the same conditions that were used to obtain the spectra shown in Figure 1 (not shown). On the other hand, this double mutant exhibited the 330 nm transition in the near UV due to the type 3 binuclear Cu(II) cluster, as well as absorbance at ~720 nm (Figure 2). This

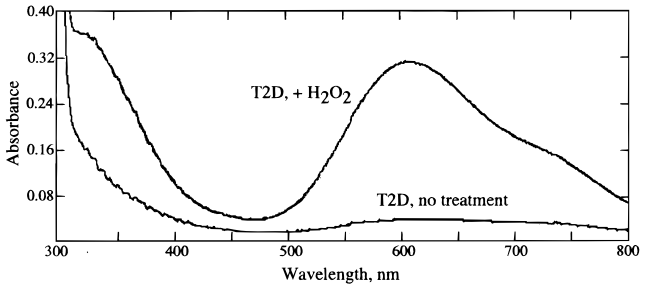

FIGURE 3: Comparison of the absorbance spectrum of the T2D mutant before and after treatment with hydrogen peroxide. The before-treatment sample (T2D, no treatment) was this mutant as obtained directly from the purification procedure. The after-treatment sample (T2D, +H_2O_2) resulted from the addition of a 10-fold molar excess of H_2O_2 followed by a 10 min incubation. The protein concentration was 4 mg/mL or 65 μM Fet3p.

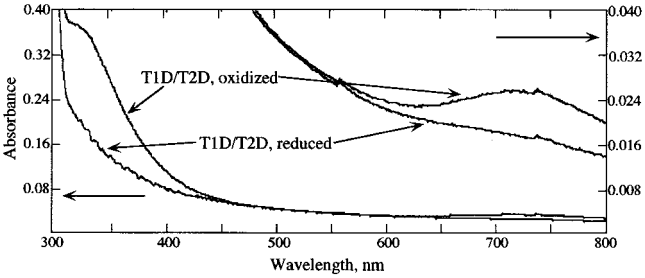

FIGURE 4: Absorbance spectrum of the oxidized and reduced forms of the T1D/T2D mutant of Fet3p. The T1D/T2D mutant as isolated was treated with hydrogen peroxide to fully oxidize the type 3 cluster. The protein was resolved from the mixture by dialysis. The resulting sample (T1D/T2D, oxidized) was at 4 mg/mL or 65 μM Fet3p in 50 mM MES buffer (pH 6.0). The other sample (T1D/T2D, reduced) was obtained following a 10 min incubation of the oxidized sample with a 10-fold molar excess of sodium dithionite followed by dialysis. The indicated oxidation−reduction cycle was repeatable (not shown).

latter result indicated that the type 3 Cu(II) site in Fet3p contributed to this absorbance in the wild-type protein (see below).

The wild-type Fet3p that was isolated was obtained in a completely oxidized state. This was shown by the fact that treatment of the protein with peroxide had no effect on the intensity of any near-UV or visible transition, or on the quantity of spins in the EPR spectrum (*11*, *12*). The same was true of the T1D mutant which, even with no peroxide treatment, gave the EPR spectrum shown in Figure 1 that is indicative of the type 2 Cu(II), and the type 3 Cu(II) 330 nm absorbance seen in Figure 2. On the other hand, both the T2D and the T1D/T2D mutants were isolated in a reduced state, as indicated by their lack of a characteristic Cu(II) EPR spectrum (as in Figure 1, T2D) and/or absorbance (as in Figure 2, T2D and T1D/T2D). However, these as-isolated, reduced samples could be readily oxidized by peroxide. This behavior is illustrated for the T2D mutant protein (Figure 3, +H_2O_2). This oxidation was reversible as indicated by the subsequent reduction with dithionite (or ascorbate) as shown for the T1D/T2D mutant in Figure 4. Figure 4 also demonstrates clearly that the type 3 Cu(II) binuclear cluster in Fet3p absorbs at ~720 nm (expanded scale, right axis). The molar extinction coefficient for this transition in the oxidized T1D/T2D mutant was determined to be 300 M^{-1} cm^{-1}. In the spectra of the wild type (and T2D proteins), this absorbance appeared as a shoulder on the more intense

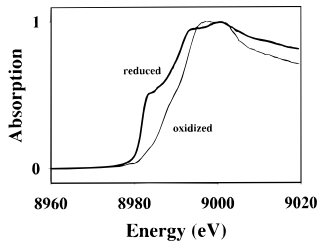

FIGURE 5: X-ray absorption edges of the reduced and oxidized forms of the T1D/T2D mutant of Fet3p. See Experimental Procedures for details.

607 nm type 1 Cu(II) feature (Figure 2), making determination of the intensity of this transition in those two cases imprecise. However, a value of 600 M^{-1} cm^{-1} was estimated, or twice that for the transition(s) assigned to the type 3 cluster alone (above), suggesting that in the native protein, the type 1 and type 3 Cu(II) sites make similar contributions to the absorbance in this region of the visible spectrum.

Significantly, the reduced forms of both the T2D and double mutant proteins were stable in air, indicating that the type 2 copper atom that was lacking in each was required for electron transfer from any of the other copper atoms in the protein to dioxygen. This result was consistent with current models for the mechanism of action of the multinuclear copper oxidases that is based on the binding of O_2 to the type 2 and one of the type 3 copper atoms (ref *34* and below).

X-ray Absorption Spectra of the T1D/T2D Fet3 Protein. The primary objective of this study was to prepare a Fet3 protein in which the type 3 binuclear copper cluster would be the sole contributor to XAS. This would allow for the use of this spectroscopic technique in the delineation of the structure of this copper site in Fet3p and enable its comparison to this site in AO, hCp, and Lac, proteins whose crystal structures have been determined.

Edge Absorption Analysis of Oxidized and Reduced T1D/T2D Fet3p. XAS data were collected on both the oxidized and reduced forms of the T1D/T2D mutant protein. Figure 5 compares the K absorption edges for these two forms. The expected difference in edge energy is clearly visible, with the oxidized enzyme exhibiting a nearly featureless edge with a midpoint energy of 8990 eV typical of tetragonally coordinated type 2 Cu(II) centers. The reduced enzyme absorbs at lower energy with a midpoint energy of 8987 eV. Furthermore, the edge exhibits a pronounced shoulder at 8984 eV that can be assigned to the $1s \rightarrow 4p_z$ plus ligand shakedown transition that acts as a marker for the coordination number in Cu(I) sites (*35*, *36*). The intensity of the shoulder at 8984 eV is characteristic of a three-coordinate site with a significant doming of the Cu(I) out of the trigonal plane, and correlates well with Cu(I) complexes in which a weakly bound fourth ligand provides a distortion toward C_{3v} symmetry.

EXAFS of Reduced T1D/T2D Fet3p. We first examined Fourier-filtered (FF) data for evidence of splitting of the first-shell distances. Three-coordinate sites are expected to have Cu−N/O distances in the range of 1.93−1.95 Å, whereas four-coordinate sites are expected to have Cu−N/O distances of >2.00 Å. We began by investigating single-shell fits in which the coordination number (*N*), the distance (*R*), and the Debye−Waller factor (DW, $2\sigma^2$) were all allowed to float. The best fit converged to an *F* value of 0.68 with an *N* of 2.8, an *R* of 2.00 Å, and a DW of 0.0124 $Å^2$. Because the high value of the DW term could be suggestive of a splitting of the first-shell distance, we next investigated two-shell fits in which the occupancy of the shells was fixed at $2N + 1N$, but *R* and DW were allowed to float freely. This gave a slightly improved fit ($F = 0.6$) consisting of 2N/O with *R* values (DW) of 1.96 Å (0.0060 $Å^2$) and 2.08 Å (0.0013 $Å^2$), respectively. Although the DW values in this fit were more reasonable for first-shell distances, the improvement in *F* was not significant. Most likely, the DW terms indicate heterogeneity between the six Cu−N (imidazole) distances characteristic of the reduced Fet3p binuclear site.

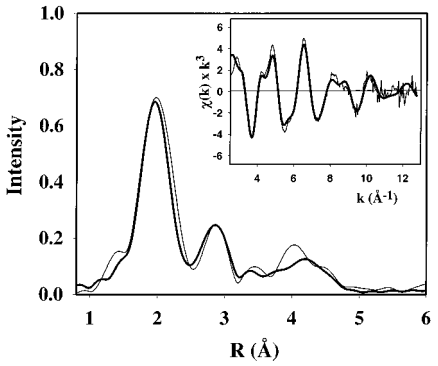

FIGURE 6: Experimental (thin lines) and simulated (thick lines) Fourier transform and EXAFS (inset) data for the reduced form the T1D/T2D mutant of Fet3p.

Table 1: Parameters Used To Simulate the EXAFS and Fourier Transform of the Reduced and Oxidized Forms of the Fet3p T1DT2D Double Mutant[a]

first shell			outer shells			
					Cu−N_a−X	
shell	*R* (Å)	$2\sigma^2$ ($Å^2$)	shell	*R* (Å)	(deg)	$2\sigma^2$ ($Å^2$)
Reduced, $F = 0.472$, $E_0 = -3.06$						
3 N(imid)	1.99	0.013	3 C(imid)	2.93	236	0.013
			3 C(imid)	3.01	130	0.013
			3 C/N(imid)	4.20	201	0.037
			3 C/N(imid)	4.27	164	0.037
1 O/N	2.49	0.021				
Oxidized, $F = 0.254$, $E_0 = -5.23$ eV						
3 N(imid)	2.04	0.014	3 C(imid)	2.96	236	0.03
			3 C(imid)	3.06	126	0.03
			3 C/N(imid)	4.22	202	0.03
			3 C/N(imid)	4.18	162	0.03
1 O(bridge)	1.91	0.008				
1 Cu	3.33	0.016				

[a] Estimated errors in distances are ±0.01 Å for the first shell and ±0.03 Å for outer shells. Estimated errors in coordination numbers are ±25%. Estimated errors in angles are ±5°.

The first-shell analysis, nonetheless, was consistent with the absorption edge data which indicated that in the reduced binuclear cluster each Cu(I) was three-coordinate. To further substantiate this conclusion, we proceeded with an exact simulation of the raw data, including single and multiple scattering contributions from coordinated histidine (imidazole) ligands. This procedure can provide good evidence for the number of such ligands (*37*, and references therein). The best fit from such a simulation is shown in Figure 6 with the parameters given in Table 1. The outer-shell scattering was well-represented with 3 N(imid) at 1.99 Å ($2\sigma^2 = 0.013$),

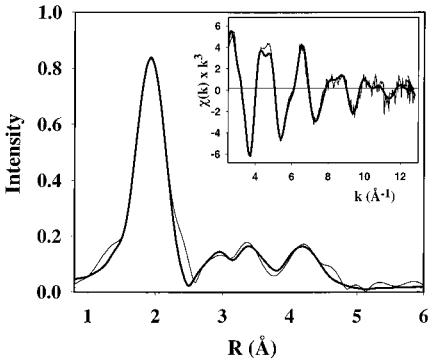

FIGURE 7: Experimental (thin lines) and simulated (thick lines) Fourier transform and EXAFS (inset) data for the oxidized form the T1D/T2D mutant of Fet3p.

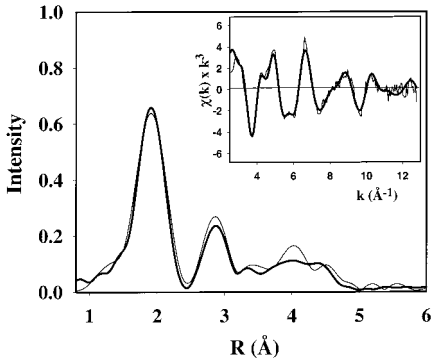

FIGURE 8: Experimental (thin lines) and simulated (thick lines) Fourier transform and EXAFS (inset) data for the reduced form the T1D mutant of Fet3p.

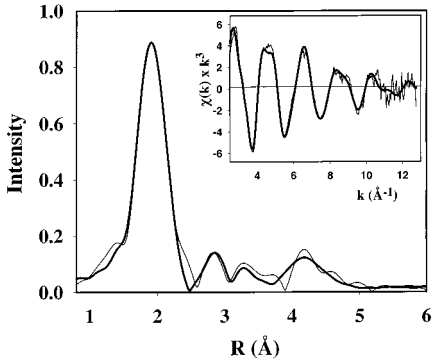

FIGURE 9: Experimental (thin lines) and simulated (thick lines) Fourier transform and EXAFS (inset) data for the oxidized form the T1D mutant of Fet3p.

although simulation of the full width of the first shell required an additional O/N at 2.49 Å ($2\sigma^2 = 0.021$). Simulations in which the first shell was split into an average of 2 N(imid) at 1.93 Å (0.007) and 1 N(imid) at 2.05 Å (0.001) also gave an acceptable fit, but the *F* value (0.59) was greater than the simple one-shell fit, providing no justification for the splitting. No Cu−Cu interaction in the *R* range of 2.5−4.0 Å could be detected by this analysis.

EXAFS of Oxidized T1D/T2D Fet3p. A first-shell FF analysis also was carried out with the data obtained for the oxidized T1D/T2D mutant. Best fits were obtained with 4 N/O scatters at 2.01 Å ($F = 0.32$), but as for the reduced enzyme, this one-shell fit gave a large DW ($2\sigma^2 = 0.017$ Å^2). These results were further refined by including multiple scattering from the imidazole rings of coordinated histidine residues. This allowed us to assign low *Z* scatters to N (imid) or O (solvent) on the basis of whether that shell had an associated set of outer-shell scatterers at the appropriate distances for an imidazole ring. Once these latter scatterers were assigned, additional first-shell scatterers (solvent) were added and allowed to float freely in the fit. This led to the simulation shown in Figure 7 with the parameters given in Table 1. The inclusion of outer-shell interactions with appropriate constraints led to an excellent fit ($F = 0.25$) with 3 N(imid) at 2.03 Å. To complete the average four-coordinate case suggested by the first-shell analysis, we included a shell of 1 O (solvent) that refined (when floated freely) to 1.91 Å. The DW terms for the histidine shells were large ($2\sigma^2 = 0.014$ Å^2), but fits that split the histidine shell ($2N + 1N$) gave no improvement in *F*. We conclude that the large DW terms arise from heterogeneity among the six Cu−N(imid) bond lengths in the oxidized type 3 cluster.

Last, the *F* value for this fit was reduced from 0.35 to 0.25 by the inclusion of a Cu−Cu interaction at 3.33 Å. This marked improvement indicates that the Cu−Cu bond distance is well-defined in the oxidized T1D/T2D protein and suggests the presence of a bridging ligand. The low *Z* scatterer (O) at 1.91 Å is a good candidate for a hydroxy bridge between the two copper atoms. This bridge has been implicated in mediating the antiferromagnetic coupling between the Cu(II) in the type 3 site in multinuclear copper oxidases. Thus, our data indicate that this site in Fet3p conforms in all general respects to the homologous site in the other members of this enzyme class.

Reduced and Oxidized T1D Fet3p. The T1D protein has an intact trinuclear cluster, and thus, all three copper atoms in the cluster contribute to the EXAFS. Because of these overlapping EXAFS contributions, spectral simulation cannot readily help to resolve meaningful differences between the coordination of any one of the three copper centers. However, one can obtain an average coordination at each copper that can be compared to the results described above. This comparison can indicate whether the removal of the type 2 Cu(II) in the T1D/T2D mutant alters the coordination at the type 3 site. Figures 8 and 9 show the best fit simulations for the reduced and oxidized T1D protein, respectively (fitted parameters in Table 2). The reduced enzyme can be well fit with 2.7 N(imid) [the average of 3 His ligated to 3 Cu(I) centers] at 1.96 Å. Oxidized T1D could be well fit with 2.7 N(imid) scatterers at 2.02 Å, 1 O at 1.89 Å, and a Cu−Cu interaction at 3.22 Å. The 0.1 Å decrease in the Cu−Cu distance in the T1D protein in comparison to that in the T1D/T2D one appeared to be significant since the Cu−Cu peak was well-defined in both mutants. No evidence was found for a 2.5 Å scatterer in the reduced T1D protein in contrast to the O/N found at 2.49 Å in the reduced T1D/T2D mutant (above). This latter scatterer could arise from the remaining "free" histidine imidazole present in the type 2 site in the double mutant protein. This and other possibilities are discussed below.

DISCUSSION

Single "deletion mutants" have been generated previously at the type 1 and type 2 copper sites in multinuclear copper oxidases by chemical means. Thus, metal substitution at the type 1 copper, e.g., mercury, to yield T1Hg Lac (*38*), or metal depletion by chelation in the presence of a reducing agent

Table 2: Parameters Used To Simulate the EXAFS and Fourier Transform of the Reduced and Oxidized Forms of the Fet3p T1D Mutant[a]

first shell			outer shells			
					Cu−N_a−X	
shell	R (Å)	$2\sigma^2$ (Å^2)	shell	R (Å)	(deg)	$2\sigma^2$ (Å^2)
Reduced, $F = 0.541$, $E_0 = -3.18$						
2.7 N(imid)	1.96	0.013	2.7 C(imid)	2.92	235	0.013
			2.7 C(imid)	2.98	130	0.013
			2.7 C/N(imid)	4.10	201	0.020
			2.7 C/N(imid)	4.31	164	0.020
Oxidized, $F = 0.279$, $E_0 = -4.61$ eV						
2.7 N(imid)	2.024	0.011	2.7 C(imid)	2.98	237	0.027
			2.7 C(imid)	3.01	126	0.027
			2.7 C/N(imid)	4.19	202	0.040
			2.7 C/N(imid)	4.13	162	0.040
1 O(bridge)	1.89	0.005				
0.5 Cu	3.22	0.013				

[a] Estimated errors in distances are ±0.01 Å for the first shell and ±0.03 Å for outer shells. Estimated errors in coordination numbers are ±25%. Estimated errors in angles are ±5°.

as in the preparation of T2D forms of Lac (*39*) and AO (*40*), has been used to generate protein forms that lacked one of the copper sites. Here, we report for the first time the use of recombinant DNA technology in generating true site-specific deletion mutants at the copper sites in a multinuclear copper oxidase. Most significantly, we also report for the first time the generation of a double mutant in which the type 3 binuclear cluster is the only site remaining. Clearly, the Fet3p system offers to provide unique protein species that can be used to test specific hypotheses about the structure and the function of this class of copper proteins. Site-directed mutagenesis has been used in the fungal laccase system; however, the mutations introduced did not cause loss of copper binding properties (*41*, *42*), although in one instance the coordination of the type 1 Cu(II) was altered (*42*).

One significant outcome of studies on the single mutants is confirmation of the sequence alignments used to suggest the identity of protein ligands to the type 1 and type 2 copper atoms in Fet3p. Absorbance and EPR data for the wild-type protein had already confirmed the prediction that Fet3p was a multinuclear copper oxidase (*11*, *12*). The mutagenesis that resulted in the specific loss of either (or both) of the EPR-detectable Cu(II) atoms in the wild-type protein is strong evidence for the correctness of the ligand assignments shown in Schemes 1 and 2. Furthermore, the near-UV and visible absorption properties of the Cu(II) atoms remaining in either single mutant protein were very similar to those of the wild type. This close similarity, if not identity, indicated that the overall structure of the two single mutant proteins was not markedly perturbed. Also, there were only small differences in the g and A values (Figure 1 and the text), consistent with little change in the electronic structure of the remaining Cu(II) site in these two single-mutant proteins. This result was similar to what has been observed in the T1Hg (*38*, *43*, *44*) and T2D Lac (*39*) and T2D AO (*40*) species. Also, the type 3 binuclear Cu(II) cluster in the T1D/T2D Fet3 protein exhibited a comparable near-UV absorption, as well as absorbance at ~720 nm. The EXAFS analysis also indicated that this cluster in the T1D and T1D/T2D mutants was very similar in overall coordination with only subtle bond length differences indicated by the fits. We interpret these results to indicate that the double mutant was also wild type in overall conformation with a "normal" type 3 cluster. Although our objective in these studies was to generate this latter mutant to isolate the type 3 cluster for XAS studies, the T1D and T2D single mutants also afforded the isolation of the individual paramagnetic copper centers. Indeed, we have initiated companion studies of these proteins by a variety of techniques, including ESEEM and MCD. The latter technique may help to assign the small spectral differences noted above to specific changes in the electronic structure of the remaining copper sites in the three mutant proteins.

As expected, none of the mutant proteins exhibited catalytic activity, including with Fe(II) as the substrate. This latter result was important inasmuch as Fet3p, and Cp, in contrast to Lac and AO, exhibit the ferroxidase reaction (eq 1) that is the apparent molecular basis for the role(s) the former two enzymes play in iron homeostasis in their respective organisms (*6*, *7*). However, despite the lack of turnover capability, the mutant proteins were redox active; in other words, the remaining copper sites could be reversibly reduced and oxidized. We did not investigate this redox process in detail, but two features are important to note here. First, the reduced forms of the T2D and T1D/T2D mutants were stable in air, while those of wild type and the T1D mutant were not. This result was completely consistent with a current model for dioxygen turnover by multinuclear copper oxidases that has the type 2 Cu(I) as one of the "tethers" for O_2 binding and subsequent electron transfer from the other Cu(I) sites in the protein (*16*). The relative inertness of T2D forms of Lac (*35*) and AO (*45*) in the reduced state toward O_2 has been observed previously.

The second important redox feature was the fact that the T2D and T1D/T2D mutant forms of Fet3p were isolated in the overall Cu(I) state while the wild-type and T1D proteins were isolated completely oxidized. One reasonable explanation for this contrasting behavior is the fact that Fet3p is produced in the yeast cell in the reduced state. Subsequently, only those protein forms that can react (turnover) with dioxygen, i.e., only those with an intact trinuclear cluster, will be oxidized within or upon release from the vesicular pathway in which the metalation of the apoFet3p occurs. What is appealing about this hypothesis is its consistency with the mechanism for trafficking of cellular copper into this vesicular pathway that most likely involves the shuttling of Cu(I) rather than Cu(II) (*46*−*48*). That is, we believe the reduced T2D or T1D/T2D Fet3p that we isolate signals the redox state of the copper that was inserted into the apoprotein in the cell. Note that we found no evidence that the growth medium had the capacity to reduce any of the Cu(II) sites in wild-type or mutant forms of Fet3p.

The most precise structural information about the type 3 site (and by extension, the trinuclear cluster) in a multinuclear copper oxidase has come from the crystal structures of hCp (*13*, *14*) and AO (*18*, *19*), and, more recently, from the crystal structure of the T2D form of a fungal laccase (*20*). The data for AO, in particular, have been most intriguing with regard to the mechanism by which dioxygen is bound and then reduced at this site (*19*). These structural studies have delineated the differences between the oxidized and reduced states of the trinuclear cluster. Most significantly, the bridging O seen in oxidized AO is lost upon reduction and the type 3 Cu−Cu distance increases from 3.7 to 5.1 Å. Upon

Scheme 3

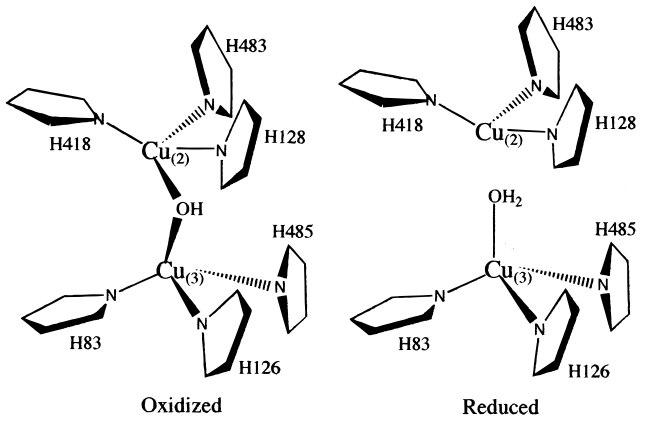

reduction and the concurrent loss of the bridging ligand, the coordination goes from a tetragonal to a trigonal planar geometry in which the 2 Cu(I) atoms are inequivalent with respect to their respective Cu−N (imidazole) bond lengths. Our EXAFS data are fully consistent with these observations with AO, indicating a similar pattern of coordination change upon reduction of the dinuclear cluster in Fet3p.

On the other hand, one aspect of our fit is more ambiguous. The data for the reduced T1D/T2D protein were best fit by including a first-shell, N/O scatterer at 2.49 Å. The data for the reduced T1D mutant [which retains the T2 Cu(I)] were well fit without this scatterer. One explanation for this difference is that in the T1D/T2D protein, which lacks His81 and the type 2 copper, the remaining histidine, His416, forms a long, yet first-shell interaction with one of the type 3 copper atoms. This ligand sphere reorganization at the binuclear cluster has been observed in the T2D form of *Coprinus cinereus* laccase (*20*). However, since all three copper atoms of the trinuclear cluster are contributing to the EXAFS of the reduced T1D protein, the fit would be relatively insensitive to a contribution of a single scatterer at only one of the copper atoms and thus not reveal the presence of an apical ligand to one of the type 3 Cu(I) atoms. Thus, an alternative explanation could be that the 2.5 Å scatterer identified in the reduced T1D/T2D is not His416 but is an apically coordinated H_2O. Its presence in the T1D mutant may simply be unable to be resolved by EXAFS. Also, its occupancy of a coordination site in the binuclear cluster in the T1D/T2D mutant could be enhanced by H-bonding to His416 that in the T1D mutant is coordinating the type 2 Cu(I). This interpretation of the EXAFS data which puts an H_2O at one of the type 3 Cu(I) atoms is consistent with the K edge shoulder at 8984 eV characteristic of trigonal Cu(I) with distinct doming toward a weakly coordinating apical ligand. This model is also appealing because of what it suggests about the mechanism of O_2 turnover at the trinuclear site.

The data for the structure of the peroxide complex with oxidized AO are informative with respect to the structure of the peroxide-level intermediate in dioxygen turnover. The peroxide is seen ligated end-on to one of the two type 3 Cu(II) atoms in the AO−peroxide complex, while the oxygen normally seen bridging the Cu(II) in the oxidized cluster is absent. The Cu−Cu distance, at 4.8 Å, is intermediate between that found in the oxidized and reduced forms (values given directly above). Thus, the data for both reduced AO and for the peroxide complex indicate the inequivalence of the copper atoms in the binuclear cluster; in the crystallographic analysis, the peroxide-bound copper was designated $Cu_{(2)}$ and its partner in the binuclear cluster, $Cu_{(3)}$.

This notation can be applied to the binuclear cluster from Fet3p using the sequence alignment shown in Scheme 2. If we assume in Fet3p that the peroxy intermediate bridges the type 2 Cu with $Cu_{(2)}$, the putative H_2O in the reduced enzyme inferred from the EXAFS data would thereby be coordinated to $Cu_{(3)}$. This model for Fet3p is shown in Scheme 3.

The presence of an oxygenous ligand coordinated to one of the type 3 Cu(I) atoms in the reduced state of the wild-type protein, as is possibly the case in the T1D/T2D mutant, would be a novel finding. Such a ligand was not fit in the electron density map for reduced AO (*19*). As illustrated in Scheme 3, we propose that the N/O ligand indicated by our fit could be a water molecule, perhaps resulting from the protonation of the bridging O(H) upon reduction of the oxidized binuclear cluster. On the basis of the AO data, and as indicated in Scheme 3 (reduced form), we propose that this water molecule is bound to $Cu_{(3)}$ and is positioned to catalyze the two-electron reduction of O_2 to HO_2^- that occurs at the type 2 (and other type 3) Cu(I). This water molecule would provide essential acid catalysis in the electron transfer to dioxygen that is tethered to the type 2 copper atom that is essential for dioxygen reduction. Hydrogen bonding of this H_2O to the dioxygen in the reduced enzyme−substrate complex leading to the peroxy intermediate would stabilize this water binding at $Cu_{(3)}$ much as we propose His416 may do in the reduced T1D/T2D mutant protein.

In summary, we have constructed the first T1D/T2D mutant of a multinuclear copper oxidase. The success of the mutant construction essentially confirms the ligand assignments in Fet3p, as in Scheme 1, based on sequence alignments among the members of this enzyme class. With this double mutant, we have obtained unique visible absorption and XAS data for the type 3 site in one of these proteins. These data indicate that the binuclear cluster in Fet3p is similar to that in hCp, AO, and laccase, and furthermore, they suggest that the dioxygen binding site that includes the type 2 copper is structurally similar as well. Last, these data confirm that the various single and double (and triple) copper site mutants we have constructed in Fet3p will enable us to test specific models of the structure and function of this enzyme in its essential role in iron homeostasis in yeast.

ACKNOWLEDGMENT

We gratefully acknowledge the use of facilities at the Stanford Synchrotron Radiation Laboratory (SSRL), which is supported by the National Institutes of Health Biomedical Research Technology Program, Division of Research Resources, and by the Department of Energy [Basic Energy Sciences (BES) and Office of Biological and Environmental Research (OBER)]. The mutant proteins described herein are based on the initial work of Dr. Daniel Yuan (The Johns Hopkins University, Baltimore, MD) and the subsequent construction of the mutant *FET3* alleles by Ms. Annette Romeo (State University of New York at Buffalo). Their contributions to this research are gratefully acknowledged.

REFERENCES

1. Askwith, C., Eide, D., Van Ho, A., Bernard, P. S., Li, L., Davis-Kaplan, S., Sipe, D. M., and Kaplan, J. (1994) *Cell 76*, 403−410.

2. de Silva, D. M., Askwith, C. C., Eide, D., and Kaplan, J. (1995) *J. Biol. Chem. 270*, 1098−1101.
3. Yuan, D. S., Stearman, R., Dancis, A., Dunn, T., Beeler, T., and Klausner, R. D. (1995) *Proc. Natl. Acad. Sci. U.S.A. 92*, 2632−2636.
4. de Silva, D., Davis-Kaplan, S., Fergestad, J., and Kaplan, J. (1997) *J. Biol. Chem. 272*, 14208−14213.
5. Stearman, R., Yuan, D. S., Yamaguchi-Iwai, Y., Klausner, R. D., and Dancis, A. (1996) *Science 271*, 1552−1557.
6. Askwith, C. C., de Silva, D., and Kaplan, J. (1996) *Mol. Microbiol. 20*, 27−34.
7. Osaki, S. (1966) *J. Biol. Chem. 241*, 5053−5059.
8. Osaki, S., Johnson, D. A., and Frieden, E. (1966) *J. Biol. Chem. 241*, 2746−2751.
9. Frieden, E., and Hsieh, H. S. (1976) in *Iron and Copper Proteins* (Yasunobu, K. T., and Mower, H. F., Eds.) Vol. 74, pp 89−244, Plenum, New York.
10. Miyajima, H., Takahashi, Y., Serizawa, M., Kaneko, E., and Gitlin, J. D. (1996) *Free Radical Biol. Med. 20*, 757−760.
11. Kosman, D. J., Hassett, R., Yuan, D. S., and McCracken, J. (1998) *J. Am. Chem. Soc. 120*, 4037−4038.
12. Hassett, R. F., Yuan, D. S., and Kosman, D. J. (1998) *J. Biol. Chem. 273*, 23274−23282.
13. Zaitseva, I., Zaitsev, V. N., Card, G., Moshkov, J., Bax, B., Ralph, A., and Lindley, P. F. (1996) *JBIC, J. Biol. Inorg. Chem. 1*, 15−23.
14. Lindley, P., Card, G., Zaitseva, I., Zaitsev, V. N., Reinhammer, B., Selin-Lindgren, E., and Yoshida, K. (1997) *JBIC, J. Biol. Inorg. Chem. 2*, 454−463.
15. Messerschmidt, A., and Huber, R. (1990) *Eur. J. Biochem. 187*, 341−352.
16. Solomon, E. I., Sundaram, U. M., and Machonkin, T. E. (1996) *Chem. Rev. 96*, 2563−2605.
17. Solomon, E. I., and Lowery, M. D. (1993) *Science 259*, 1575−1581.
18. Messerchmidt, A., Ladenstein, R., Huber, R., Bolognesi, M., Avigliano, L., Petruzzelli, R., Rossi, A., and Finazzi-Agró, A. (1992) *J. Mol. Biol. 224*, 179−205.
19. Messerschmidt, A., Luecke, H., and Huber, R. (1993) *J. Mol. Biol. 230*, 997−1014.
20. Ducros, V., Brzozowski, A. M., Wilson, K. S., Brown, S. H., Ostergaard, P., Schneider, P., Yaver, D. S., Pedersen, A. H., and Davies, G. J. (1998) *Nat. Struct. Biol. 5*, 310−316.
21. Co, M. S., and Hodgson, K. O. (1984) in *Copper Proteins and Copper Enzymes* (Lontie, R., Ed.) Vol. I, pp 93−113, CRC Press, Boca Raton, FL.
22. Yamaguchi-Iwai, Y., Dancis, A., and Klausner, R. D. (1995) *EMBO J. 14*, 1231−1239.
23. Yamaguchi-Iwai, Y., Stearman, R., Dancis, A., and Klausner, R. D. (1996) *EMBO J. 15*, 3377−3384.
24. Bradford, M. M. (1976) *Anal. Biochem. 72*, 248−254.
25. Smith, P. K., Krohn, R. I., Hermanson, G. T., Mallia, A. K., Gartner, F. H., Provenzano, M. D., Fujimoto, E. K., Goeke, N. M., Olson, B. J., and Klenk, D. C. (1985) *Anal. Biochem. 150*, 76−85.
26. Bonomi, F., Kurtz, D. M., Jr., and Cui, X. (1996) *JBIC, J. Inorg. Biol. Chem. 1*, 67−72.
27. George, G. N. (1990) http:/ssrl.stanford.edu/exafspak.html.
28. Gurman, S. J. (1989) in *Synchrotron Radiation and Biophysics* (Hasnain, S. S., Ed.) pp 9−42, Ellis Horwood Ltd., Chichester, United Kingdom.
29. Gurman, S. J., Binsted, N., and Ross, I. (1984) *J. Phys. C 17*, 143−151.
30. Gurman, S. J., Binsted, N., and Ross, I. (1986) *J. Phys. C 19*, 1845−1861.
31. Blackburn, N. J., Hasnain, S. S., Pettingill, T. M., and Strange, R. W. (1991) *J. Biol. Chem. 266*, 23120−23127.
32. Sanyal, I., Karlin, K. D., Strange, R. W., and Blackburn, N. J. (1993) *J. Am. Chem. Soc. 115*, 11259−11270.
33. Strange, R. W., Blackburn, N. J., Knowles, P. F., and Hasnain, S. S. (1987) *J. Am. Chem. Soc. 109*, 7157−7162.
34. Shin, W., Sundaram, U. M., Cole, J. L., Zhang, H. H., Hedman, B., Hodgson, K. O., and Solomon, E. I. (1996) *J. Am. Chem. Soc. 118*, 3203−3215.
35. Kau, L.-S., Spir-Solomon, D. J., Penner-Hahn, J. E., Hodgson, K. O., and Solomon, E. I. (1987) *J. Am. Chem. Soc. 109*, 6433−6442.
36. Blackburn, N. J., Strange, R. W., Reedjik, J., Volbeda, A., Farooq, A., Karlin, K. D., and Zubieta, J. (1989) *Inorg. Chem. 28*, 1349−1357.
37. Ralle, M., Verkovskaya, M. L., Morgan, J. E., Verkovsky, M. I., Wikström, M., and Blackburn, N. J. (1999) *Biochemistry 38*, 7185−7194.
38. Klemens, A. S., McMillin, D. R., Tsang, H. T., and Penner-Hahn, J. E. (1989) *J. Am. Chem. Soc. 111*, 6398−6402.
39. Eggleston, M. K., Pecoraro, C., and McMillin, D. R. (1995) *Arch. Biochem. Biophys. 320*, 276−279.
40. Messerschmidt, A., Steigemann, W., Huber, R., Lang, G., and Kroneck, P. M. H. (1992) *Eur. J. Biochem. 209*, 597−602.
41. Xu, F., Berka, R. M., Wahleithner, J. A., Nelson, B. A., Shuster, J. R., Brown, S. H., Palmer, A. E., and Solomon, E. I. (1998) *Biochem. J. 334*, 63−70.
42. Xu, F., Palmer, A. E., Yaver, D. S., Berka, R. M., Gambetta, G. A., Brown, S. H., and Solomon, E. I. (1999) *J. Biol. Chem. 274*, 12372−12375.
43. Cole, J. L., Clark, P. A., and Solomon, E. I. (1990) *J. Am. Chem. Soc. 112*, 9534−9548.
44. Lu, J., Bender, C. J., McCracken, J., Peisach, J., Severns, J. C., and McMillin, D. R. (1992) *Biochemistry 31*, 6265−6272.
45. Avigliano, L., Desideri, A., Urbanelli, S., Mondovi, B., and Marchesini, A. (1979) *FEBS Lett. 231*, 318−320.
46. Pufahl, R. A., Singer, C. P., Peariso, K. L., Lin, S.-J., Schmidt, P. J., Fahrni, C. J., Culotta, V. C., Penner-Hahn, J. E., and O'Halloran, T. V. (1997) *Science 278*, 853−856.
47. Lutsenko, S., Petrukhin, K., Copper, M. J., Gilliam, C. T., and Kaplan, J. H. (1997) *J. Biol. Chem. 272*, 18939−18944.
48. Ralle, M., Cooper, M. J., Lutsenko, S., and Blackburn, N. J. (1998) *J. Am. Chem. Soc. 120*, 13525−13526.

BI992334A